Am. J. Hum. Genet. 74:128–138, 2004

Mutation of *CERKL,* a Novel Human Ceramide Kinase Gene, Causes Autosomal Recessive Retinitis Pigmentosa (RP26)

Miquel Tuson, Gemma Marfany, and Roser Gonzàlez-Duarte

Departament de Genètica, Facultat de Biologia, Universitat de Barcelona, Barcelona

Retinitis pigmentosa (RP), the main cause of adult blindness, is a genetically heterogeneous disorder characterized by progressive loss of photoreceptors through apoptosis. Up to now, 39 genes and loci have been implicated in nonsyndromic RP, yet the genetic bases of >50% of the cases, particularly of the recessive forms, remain unknown. Previous linkage analysis in a Spanish consanguineous family allowed us to define a novel autosomal recessive RP (arRP) locus, RP26, within an 11-cM interval (17.4 Mb) on 2q31.2-q32.3. In the present study, we further refine the RP26 locus down to 2.5 Mb, by microsatellite and single-nucleotide polymorphism (SNP) homozygosity mapping. After unsuccessful mutational analysis of the nine genes initially reported in this region, a detailed gene search based on expressed-sequence-tag data was undertaken. We finally identified a novel gene encoding a ceramide kinase (*CERKL*), which encompassed 13 exons. All of the patients from the RP26 family bear a homozygous mutation in exon 5, which generates a premature termination codon. The same mutation was also characterized in another, unrelated, Spanish pedigree with arRP. Human *CERKL* is expressed in the retina, among other adult and fetal tissues. A more detailed analysis by in situ hybridization on adult murine retina sections shows expression of *Cerkl* in the ganglion cell layer. Ceramide kinases convert the sphingolipid metabolite ceramide into ceramide-1-phosphate, both key mediators of cellular apoptosis and survival. Ceramide metabolism plays an essential role in the viability of neuronal cells, the membranes of which are particularly rich in sphingolipids. Therefore, CERKL deficiency could shift the relative levels of the signaling sphingolipid metabolites and increase sensitivity of photoreceptor and other retinal cells to apoptotic stimuli. This is the first genetic report suggesting a direct link between retinal neurodegeneration in RP and sphingolipid-mediated apoptosis.

Introduction

Inherited retinal degenerative diseases are characterized by the progressive loss of mature photoreceptor cells through apoptosis. Among them, retinitis pigmentosa (RP [MIM 268000]), the most common hereditary cause of blindness, comprises a clinically and genetically heterogeneous group of retinal disorders that affects ~1.5 million people worldwide (Sullivan and Daiger 1996). Patients with RP typically show night blindness, gradual visual impairment, and bone spicule–like pigment deposits in the retina.

RP is a paradigm of monogenic diseases with extremely high genetic heterogeneity (Hims et al. 2003). This complexity has clearly hindered the identification of causative genes, particularly in the recessive forms, since large nuclear families suitable for linkage studies are scarce. In fact, although 39 genes and loci have been described, many others, still unknown, could account for the remaining unassigned cases. At present, the reported RP causative genes fall into four categories: (*a*) genes directly involved in the phototransduction cascade, (*b*) genes encoding proteins responsible for the structure and polarity of the photoreceptors, (*c*) genes encoding proteins of the visual cycle, and (*d*) regulatory genes (such as transcription and splicing factors). In the study of autosomal recessive RP (arRP), mutations on 16 genes and linkage to five chromosomal regions have been reported (Wang et al. 2001; RetNet Web site). Therefore, RP gene identification is still a priority in this field, since it not only is needed for diagnosis but also is crucial for giving insights into the molecular basis of the disease.

RP26, one of the remaining uncharacterized loci, was previously mapped to an 11-cM interval on 2q31.2-q32 in a consanguineous family with arRP (Bayés et al. 1998). Later, this 11-cM interval, between markers D2S148 and D2S117, was ascribed to a physical distance of 17.4 Mb that comprised more than 50 genes. As the incoming human genome data were made available in the public databases, new markers—either microsatellites or, mainly, SNPs—were retrieved and analyzed, first for cosegregation and finally for homozygosity mapping. All

Received September 5, 2003; accepted for publication October 27, 2003; electronically published December 16, 2003.

Address for correspondence and reprints: Dr. Roser Gonzàlez-Duarte, Departament de Genètica, Facultat de Biologia, Universitat de Barcelona, Av. Diagonal 645, E-08028 Barcelona, Spain. E-mail: rgonzalez@ub.edu

0002-9297/2004/7401-0013$15.00

of this new information allowed us to narrow the candidate region to 2.5 Mb, and mutational screening was subsequently performed to identify the RP26 gene.

Material and Methods

Families and DNA

The two families with arRP we analyzed, P2 and E1, have been described elsewhere (Bayés et al. 1996, 1998). Blood samples were collected from family members, and DNA was extracted using a commercial kit (Wizard Genomic DNA Purification Kit [Promega]). Informed consent was gathered from all family members. This research followed the tenets of the Declaration of Helsinki.

Cosegregation and Homozygosity Mapping

The RP26 locus was further refined using three flanking markers: D2S2978, D2S2261, and D2S273 (table 1). For subsequent homozygosity mapping, additional markers (13 microsatellites and 101 SNPs) were chosen on the basis of their physical position according to the National Center for Biotechnology Information (NCBI) Human Builds 29–33 at the University of California Santa Cruz Genome Bioinformatics Web site (table 1). The SNP sequences were retrieved from the NCBI dbSNP Home Page and The SNP Consortium database. New SNPs observed during this study were submitted and deposited in the NCBI dbSNP database (see table 1). SNP analyses involved PCR assays with flanking primers and subsequent sequencing to verify the genotype. Three amplification steps (30 s each), with the annealing temperature ranging from 48°C to 61°C, were performed. The reaction mixture (50 μl) contained 10 μM of each primer, 2 μM of dNTPs, 1.5 mM $MgCl_2$, and 1 U of *Taq* polymerase (Innogenetics).

Mutation Screening

Primers located at the flanking intron regions were designed to amplify each coding exon for all the analyzed genes in all samples. Three amplification steps (30 s each), with the annealing temperature ranging from 45°C to 60°C, were performed. Sequencing was performed using the BigDye Terminator Cycle Sequencing v3.1 kit and the automatic sequencers ABI 3700 and ABI 3730 (Applied Biosystems).

Mutation Restriction Analysis

A forward primer (5′-GAAGAATGCTGGGATGGAAACGGAC-3′) containing a mismatch nucleotide (underlined) that created an *Ava*II restriction site in the exon 5 wild-type sequence was designed. A three-step PCR (annealing temperature 50°C) was performed on the genomic DNA of the P2 and E1 family members, through use of the mismatch forward primer and exon 5 reverse primer (5′-GTTGTGCTGTCTAGATTAGC-3′), under the conditions mentioned above. The 157-bp PCR fragments were digested with *Ava*II and were resolved in a 4% low-melting-temperature agarose gel.

Human and Murine CERKL *cDNA Characterization*

Database searches from the available human genomic sequence allowed the identification of a truncated EST (GenBank accession number BE797822) and a partial cDNA (GenBank accession number BC020465), which overlapped 18 bp. To characterize the full-length cDNA, a human retina cDNA library (BD Biosciences) was screened (1.2×10^6 plaque-forming units) with a mixture of all the *CERKL* coding exons as a probe. The hybridization was performed overnight under highly stringent conditions (42°C in 50% formamide, 5 × Denhardt's, 5 × SSPE, 0.1% sodium dodecyl sulfate, and 100 μg/ml salmon sperm DNA), and several washes were performed at 55°C in 2 × SSC and 1 × SSC before autoradiography. Only a partial *CERKL* cDNA was obtained. For the full-length coding sequence, we devised a PCR strategy using two specific primers flanking the conceptual ATG and STOP codons on the Marathon-Ready retina cDNA (BD Biosciences) under the following conditions: 94°C for 30 s, 60°C for 30 s, and 72°C for 2 min for 40 cycles. The reaction mixture (50 μl) contained 10 μM of each primer, 2 μM of dNTPs, 1.5 mM $MgCl_2$, 1 U of *Taq* polymerase (Innogenetics), and 5% DMSO.

TBLASTN database searches at the NCBI BLAST server revealed two murine sequences homologous to human *CERKL,* one EST (GenBank accession number BY742285) and one partial cDNA (GenBank accession number BC046474), which had 377 nt of overlap with one another. Protein alignment was performed with CLUSTALW 1.8 at the BCM Search Launcher Web site and was depicted with BOXSHADE 3.21 at the EMBnet BoxShade Server.

Phylogenetic Analysis

Protein sequences from several members of the diacylglycerol, sphingosine, and ceramide kinase families were retrieved from public databases and aligned with human and murine CERKL through use of CLUSTALX version 1.64 (Thompson et al. 1997). The resulting phylogenetic tree was constructed using the neighbor-joining algorithm and considering the diacylglycerol kinase sequences as outgroup.

RT-PCRs

Two specific primers on exons 8 (5′-CCATTTAACAGCTCTGATGATGTGCAAG-3′) and 12 (5′-GACCTCTGATGCAACTTCCATTAAGTCAC-3′), which ampli-

Table 1

Microsatellite and SNP Markers Analyzed on 2q31.2-q32.3

Microsatellite or SNP ID[a]	Location[b]	Locus	Genotype in RP26 Patients[c]
D2S148; AFM200WA11	chr2: 176902551–176902745		Recombinant
D2S2978; ATA44H04	chr2: 179788236–179788348		Recombinant
D2S2261; AFMB072WG1	chr2: 180180111–180180442		Recombinant
rs1002207; TSC0036660	chr2: 180237706		Noninformative
rs1949453; TSC1026876	chr2: 180594170	*UBE2E3*	***Homozygous***
*rs2077783; TSC0046543	chr2: 180834855		***Homozygous***
*rs720453; TSC0046544	chr2: 180834909		***Homozygous***
*D2S2310; AFMB355XD5	chr2: 180849531–180849858		Noninformative
*rs155100; TSC0531809	chr2: 181033165	*ITGA4*	***Homozygous***
*rs155101; TSC0531810	chr2: 181033223	*ITGA4*	***Homozygous***
*rs155102	chr2: 181033525	*ITGA4*	***Homozygous***
*rs155103	chr2: 181033821	*ITGA4*	***Homozygous***
rs1801262	chr2: 181226533	*NEUROD1*	***Homozygous***
rs2583016	chr2: 181228296	*NEUROD1*	***Homozygous***
*rs1157595; TSC0326375	chr2: 181432646		***Homozygous***
*D2S364; AFM303YA9	chr2: 181717611–181718002	*PDE1A*	***Homozygous***
*rs3754929	chr2: 181771662	*PDE1A*	***Homozygous***
*rs1438065; TSC0655111	chr2: 181902071	*PDE1A*	***Homozygous***
*rs833152; TSC0655110	chr2: 181902179	*PDE1A*	Noninformative
rs288254; TSC0681111	chr2: 182291705	*ERdj5*	Noninformative
rs7510	chr2: 182472727	*NCKAP1*	Heterozygous
ss12676100	chr2: 182476461	*NCKAP1*	Heterozygous
ss12676101	chr2: 182476476	*NCKAP1*	Heterozygous
ss12676102	chr2: 182482636	*NCKAP1*	Heterozygous
rs2271671	chr2: 182510096	*NCKAP1*	Heterozygous
D2S350; AFM292WD1	chr2: 182532022–182532389	*NCKAP1*	Heterozygous
ss12676103	chr2: 182678153	LOC129401	Heterozygous
ss12676104	chr2: 182678197	LOC129401	Heterozygous
ss12676105	chr2: 182678220	LOC129401	Heterozygous
D2S2273; AFMB297XC1	chr2: 182825486–182825797		Heterozygous
D2S2281; AFMB310XF5	chr2: 182863973–182864335		Heterozygous
D2S2366; AFMA057VG9	chr2: 183175061–183175459		Noninformative
rs826135; TSC1254035	chr2: 183459257		Noninformative
rs826134; TSC0476562	chr2: 183459267		Noninformative
ss12676106	chr2: 183459509		Heterozygous
rs826133; TSC0658245	chr2: 183459526		Noninformative
ss12676107	chr2: 183459659		Heterozygous
ss12676108	chr2: 183459776		Heterozygous
rs826132; TSC0658244	chr2: 183459802		Heterozygous
D2S1391; GATA65C03	chr2: 183675508–183675835		Homozygous
rs1443021; TSC0664031	chr2: 183910062		Heterozygous
rs1443022; TSC0664032	chr2: 183910149		Heterozygous
rs768352; TSC0076040	chr2: 184012769		Homozygous
rs994653; TSC0317578	chr2: 184193063		Homozygous
rs728534; TSC0064305	chr2: 184484995		Homozygous
rs3046266; TSC1530131	chr2: 184485293		Noninformative
rs1366842; TSC0514415	chr2: 184485321		Noninformative
rs3731834	chr2: 184486442		Homozygous
D2S1361; GATA14E05	chr2: 184899775–184900087		Heterozygous
rs1016410; TSC0098979	chr2: 185334459		Heterozygous
rs1019430; TSC0223209	chr2: 185334589		Heterozygous
rs878845; TSC0212635	chr2: 185580725		Heterozygous
ss12676109	chr2: 186138356	*ITGAV*	Heterozygous
ss12676110	chr2: 186170238	*ITGAV*	Heterozygous
ss12676111	chr2: 186181185	*ITGAV*	Heterozygous
ss12676112	chr2: 186186304	*ITGAV*	Heterozygous
ss12676113	chr2: 186202416	*ITGAV*	Heterozygous
rs3816386	chr2: 186211713	*ITGAV*	Heterozygous
rs2018302; TSC0091486	chr2: 186467891		Heterozygous
rs1467990; TSC0384843	chr2: 186468012		Noninformative
rs2018314; TSC0085681	chr2: 186468088		Heterozygous
rs1000623; TSC0033486	chr2: 186468142		Heterozygous
rs840570; TSC1028023	chr2: 186855755		Noninformative
rs2308091	chr2: 186856059		Noninformative
rs84069	chr2: 186856203		Noninformative
rs84068	chr2: 186856285		Noninformative

(continued)

Table 1 (continued)

Microsatellite or SNP ID[a]	Location[b]	Locus	Genotype in RP26 Patients[c]
D2S152; AFM207XG1	chr2: 186914674–186915071	*CALCRL*	Noninformative
rs1398061; TSC0576737	chr2: 186941063	*CALCRL*	Noninformative
rs1464338; TSC0378776	chr2: 187177069		Noninformative
rs1464337; TSC0378775	chr2: 187177070		Noninformative
rs2176858; TSC1217605	chr2: 187177146		Noninformative
rs2033838; TSC1047282	chr2: 187551834		Heterozygous
rs2028374; TSC1091521	chr2: 187666577		Heterozygous
rs1354906; TSC0490640	chr2: 188129892	CED-6	Homozygous
rs1007120: TSC0084553	chr2: 188175289		Noninformative
rs925825; TSC0241755	chr2: 188431720		Heterozygous
rs893407; TSC0165376	chr2: 189033193		Heterozygous
rs2289404	chr2: 189318673	*ORMDL1*	Noninformative
rs6942; TSC0023616	chr2: 189319070	*ORMDL1*	Homozygous
rs3791767	chr2: 189322574	*ORMDL1*	Noninformative
rs288817; TSC1078112	chr2: 189529648		Noninformative
ss12676114	chr2: 189529690		Homozygous
rs998173; TSC0011271	chr2: 189694293		Homozygous
rs3791789	chr2: 189787488	*HIBCH*	Heterozygous
D2S2262; AFMB082YE1	chr2: 189985176–189985493		Heterozygous
rs7721	chr2: 190069246		Heterozygous
rs1128723	chr2: 190069374		Heterozygous
rs8962	chr2: 190074316		Noninformative
rs1468685; TSC0385949	chr2: 190268436		Heterozygous
rs1263136; TSC1488116	chr2: 190298357		Noninformative
rs1263125; TSC0446273	chr2: 190303089		Homozygous
D2S118; AFM066XC1	chr2: 190309134–190309312		Homozygous
rs1263100; TSC0398872	chr2: 190327138		Heterozygous
rs1476896; TSC0398871	chr2: 190327184		Homozygous
D2S389; AFM333WF9	chr2: 190347305–190347628		Homozygous
rs1882395; TSC0896111	chr2: 190387668		Homozygous
D2S1775; GATA71C07	chr2: 190402485–190402614		Homozygous
rs3217036	chr2: 190462343	*GLS*	Noninformative
rs2355571	chr2: 190477428	*GLS*	Heterozygous
rs2883713	chr2: 190491082	*GLS*	Heterozygous
rs3199237	chr2: 190497863	*GLS*	Noninformative
rs3207595	chr2: 190497884	*GLS*	Noninformative
rs3207596	chr2: 190497887	*GLS*	Noninformative
rs3199238	chr2: 190497893	*GLS*	Noninformative
rs3207597	chr2: 190497917	*GLS*	Noninformative
rs1801893	chr2: 190498994	*GLS*	Noninformative
rs3215259	chr2: 190521768	*GLS*	Noninformative
rs1058589	chr2: 190522002	*GLS*	Noninformative
rs1058590	chr2: 190522011	*GLS*	Noninformative
rs1058591	chr2: 190522017	*GLS*	Noninformative
rs1058592	chr2: 190522020	*GLS*	Noninformative
rs1547550; TSC0429185	chr2: 190548390	*STAT1*	Heterozygous
rs925847; TSC0241788	chr2: 190600205	*STAT4*	Noninformative
rs3024891	chr2: 190601614	*STAT4*	Heterozygous
D2S2246; AFMB007WC1	chr2: 191085514–191085746		Heterozygous
D2S318; AFM105XC1	chr2: 191278428–191278834		Homozygous
D2S161; AFM224ZF4	chr2: 191431730–191432052		Heterozygous
D2S280; AFM155YE1	chr2: 191557728–191557932	*TMEFF2*	Homozygous
rs3738882	chr2: 191751560	*TMEFF2*	Homozygous
rs935367; TSC0352562	chr2: 191842107		Noninformative
D2S315; AFM081YG5	chr2: 192076101–192076267		Homozygous
rs717621; TSC0040380	chr2: 192153621		Heterozygous
D2S273; UT5048	chr2: 192288946–192289538		Recombinant
D2S117; AFM065YF11	chr2: 194331362–194331699		Recombinant

[a] Microsatellite IDs are those that begin with "D," and SNP IDs are those that begin with "rs" or "ss." SNPs IDs that begin with "ss" are those identified in the present study and are deposited in the NCBI dbSNP database. Microsatellite and SNP IDs preceded by an asterisk (*) are the flanking *CERKL* markers used for haplotype analysis and comparison in families P2 and E1.

[b] Location in NCBI Build 32.

[c] Boldface italic type indicates candidate homozygous region.

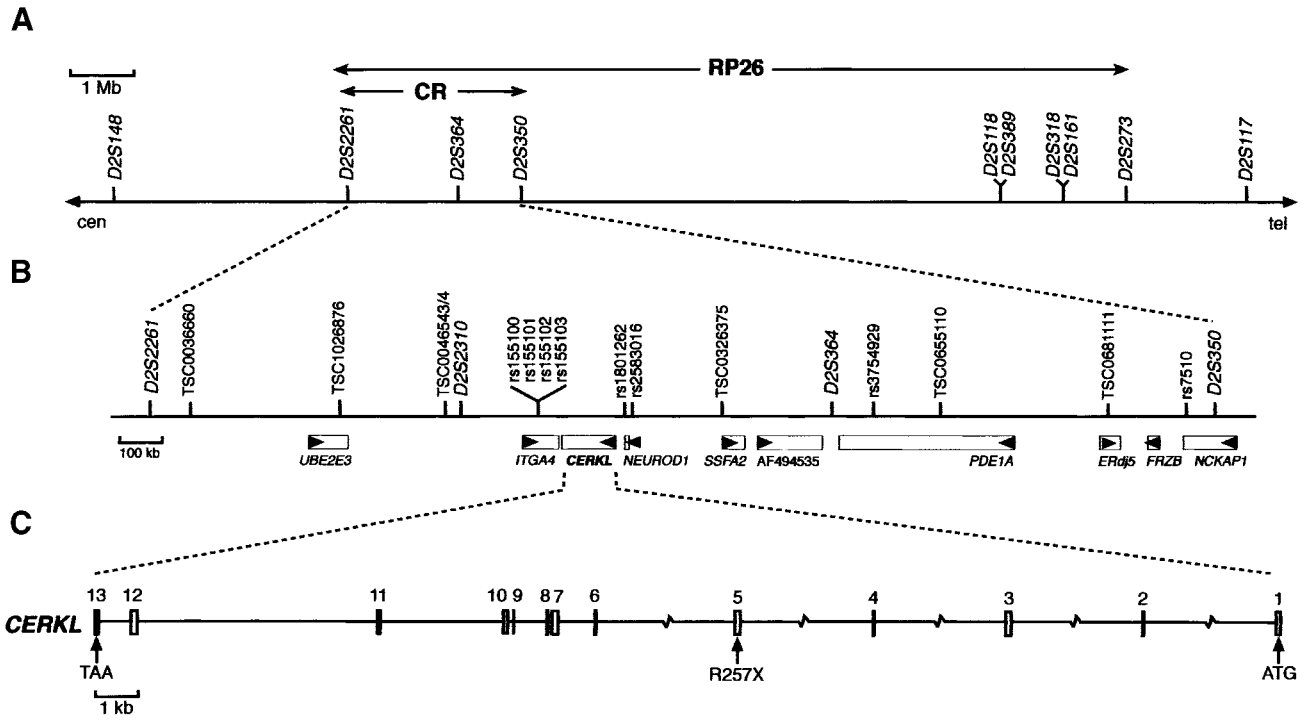

Figure 1 The RP26 locus and the *CERKL* gene and protein. *A*, RP26 physical map of the 12.5-Mb cosegregation interval between markers D2S2261 and D2S273. *B*, Localization of *CERKL* within the candidate region ("CR") defined by homozygosity mapping. Genes (*rectangles*) and the transcription direction (*arrowheads*) are indicated. *C*, *CERKL* exon/intron structure. The location of the R275X null mutation in exon 5 is shown.

fied 429 bp, were used to detect *CERKL* expression on a panel of first-strand cDNAs of several human adult and fetal tissues (BD Biosciences). Specific *CERKL* expression was confirmed by sequencing the amplified products. Amplification of *GAPD* was used to compare and normalize the samples, as suggested by the manufacturer. PCR conditions were as follows: 35 cycles of 94°C for 30 s and 65°C for 60 s. The reaction mixture (50 μl) contained 10 μM of each primer, 2 μM of dNTPs, 1.5 mM $MgCl_2$, and 1 U *Taq* pol (Innogenetics).

In Situ Hybridizations

For in situ hybridization, adult mouse eye slides from the C57BL/6J strain were obtained from Novagen. Eyes were fixed in 4% paraformaldehyde, embedded in paraffin, and sectioned at 7 μm. Sections were washed for 7 min three times with xylene to remove paraffin, for 3 min twice with ethanol 100%, for 3 min with ethanol 90%, for 3 min with ethanol 70%, and for 3 min with diethyl pyrocarbonate–treated water, and then were fixed with 4% paraformaldehyde for 20 min. Sections were treated with 2 μg/ml proteinase K for 30 min, washed for 5 min twice with phosphate-buffered saline, and postfixed with 4% paraformaldehyde. Acetylation with 0.1 M triethanolamine-HCl (pH 8.0) containing 0.25% acetic anhydride was performed for 10 min. Slides were subsequently washed, ethanol dehydrated, and air dried. Hybridization was performed overnight at 55°C with 2 μg/ml digoxigenin-labeled riboprobes in 50% formamide, 1 × Denhardt's solution, 10% dextran sulfate, 0.3 M NaCl, 10 mM Tris-HCl (pH 8.0), 5 mM EDTA (pH 8.0), 10 mM NaH_2PO_4, and 200 μg/ml salmon sperm DNA.

The riboprobes were generated from the T7 and T3 promoters of a pBluescript II KS vector containing either a 201-bp *Hin*dIII-*Pst*I fragment, a 350-bp *Hin*dIII fragment, a 513-bp *Pst*I-*Sph*I fragment of the murine *Cerkl* cDNA IMAGE 4504238, or a 198-bp fragment from coding exon 4 of murine rhodopsin.

After hybridization, the slides were washed in 2 × SSC for 20 min; washed for 5 min twice in a solution of 50% formamide and 2 × SSC (washes at 50°C); equilibrated in NTE (0.5 M NaCl, 10 mM Tris-HCl pH 8.0, 5 mM EDTA) at 37°C; and then treated with 10 μg/ml RNase A in NTE at 37°C for 30 min. Subsequently, the sections were washed in NTE, 2 × SSC, and 0.1 × SSC (15 min each), equilibrated in buffer 1 (100 mM Tris-HCl pH 7.5, 150 mM NaCl), and blocked in blocking buffer (1% BSA and 0.1% Triton X-100 in buffer 1) for 30 min. An anti-digoxigenin-AP conjugate antibody (1:500; Roche Applied Science) in blocking buffer was incubated

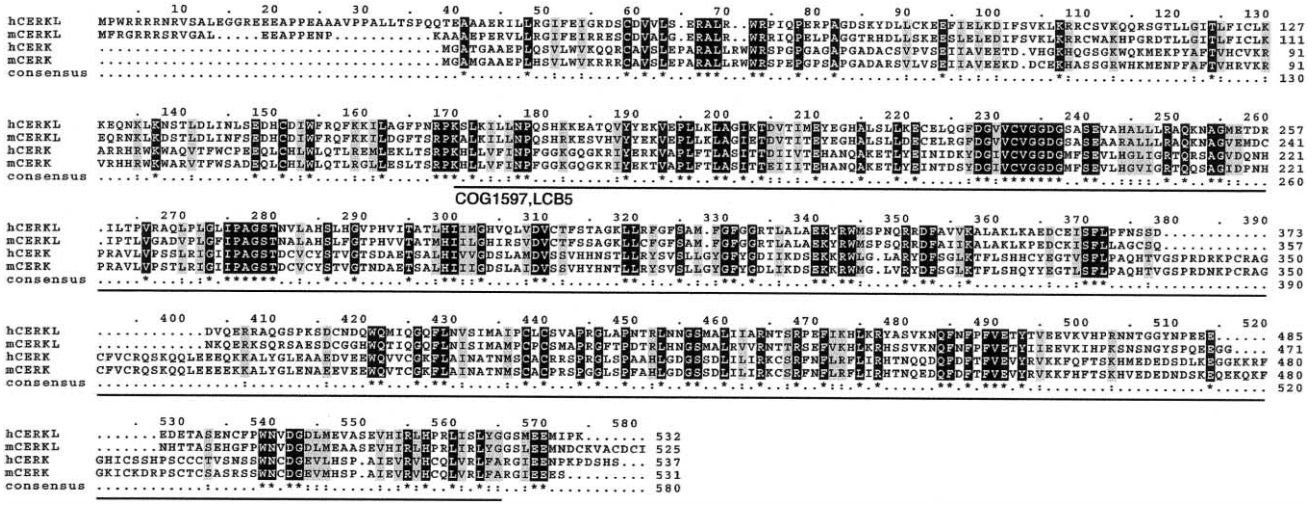

Figure 2 Protein alignment of human ("h") and murine ("m") CERKL and CERK. Identical residues are highlighted in black, and conservative positions are in gray. The solid black line underlines the conserved COG1597 (LCB5) domain detected after comparison with the NCBI Conserved Domain Database. Murine CERKL sequence was assembled from GenBank sequences BY742285 and BC046474, human CERK sequence from AB079066, and murine CERK sequence from AB79067.

overnight at 4°C. The sections were washed twice in buffer 1 for 15 min and in buffer 2 (100 mM Tris-HCl pH 9.5, 150 mM NaCl, and 50 mM $MgCl_2$) for 10 min prior to exposure to the alkaline phosphatase substrate, nitroblue tetrazolium–5-bromo-4-chloro-3-indoyl phosphate (NBT-BCIP; Roche Applied Science). The reaction was stopped by several washes in distilled water. The sections were cover-slipped with 70% glycerol in PBS and were photographed using a Nomarski optics microscope (Axioplan, Carl Zeiss) equipped with a Nikon Coolpix digital camera.

Results

Refinement of the Cosegregation Region and Candidate Gene Analysis

The analysis of two proximal (D2S2978 and D2S2261) and one distal (D2S273) flanking markers (table 1) allowed further refinement of the RP26 locus to a 12.5-Mb interval (fig. 1*A*). As a first attempt to identify the causative gene, a mutational screening of candidate genes selected on the basis of their known retinal function or the phenotype of *Drosophila* mutants or knockout mice was performed. The analysis of five candidates (*ORMDL1, ITGAV, GLS, NEUROD1,* and *FRZB*) within this interval did not reveal any pathogenic mutation.

Homozygosity Mapping and Mutation Screening

The reported consanguinity of the RP26 family and the availability of new markers after the sequencing of the human genome made homozygosity mapping feasible as a means to reduce the candidate region. Sixteen microsatellite markers and 101 SNPs located within the 12.5-Mb interval (table 1) were analyzed in all P2 family members. Eventually, only one homozygous segment spanning >1 Mb, between markers D2S2261 and D2S350 (fig. 1*A*), was identified. This candidate region, spanning 2.5 Mb, harbored five annotated genes and four partially characterized mRNAs (fig. 1*B*), which were prioritized for mutational analysis on the basis of (*a*) retinal expression, as assessed by PCR on a retina cDNA library; and (*b*) availability of functional data. All of them were eventually sequenced (in fact, two genes, *NEUROD1* and *FRZB,* were analyzed in the previous section), but none showed any pathogenic variant.

Identification of a Novel Gene, CERKL

A more exhaustive database search for uncharacterized cDNAs and spliced ESTs within the candidate 2.5-Mb region was undertaken and revealed two close sequences, one EST (GenBank accession number BE797822) and one eye/retinoblastoma incomplete cDNA (GenBank accession number BC020465), located between the *ITGA4* and the *NEUROD1* genes. The conceptual protein from the *in silico* assembly of both sequences showed homology with eukaryotic ceramide, sphingosine, and diacylglycerol kinases and strongly suggested that the sequences analyzed corresponded to a novel, unreported gene. After screening a human retina cDNA library and performing serial PCR assays on retina cDNA, we obtained the full-length 1,596-nt coding sequence, which spanned 13 exons (fig. 1*C*). The predicted 532-aa protein showed the highest similarity (29% identity; 50% similarity) with the human

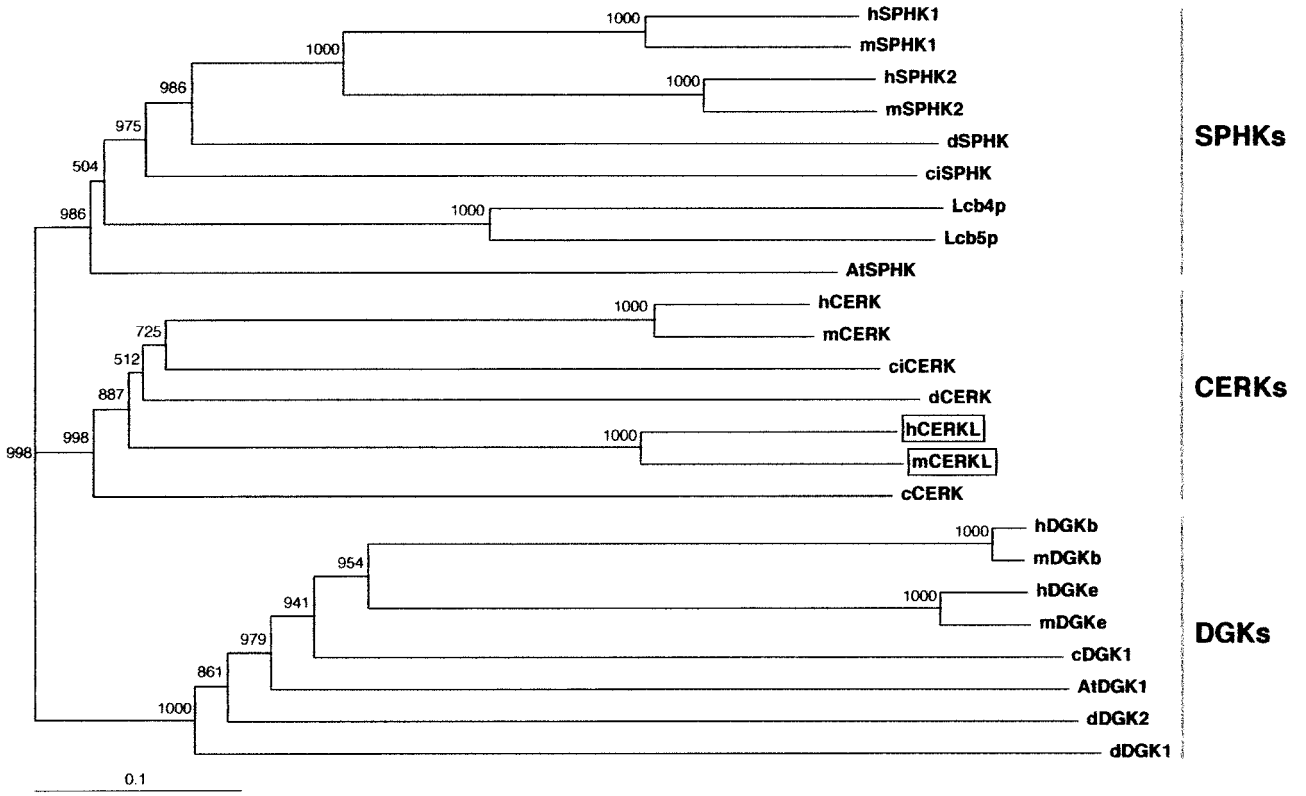

Figure 3 Unrooted phylogenetic tree of several members of the diacylglycerol, sphingosine, and ceramide kinases, including the human and murine CERKL sequences described in the present study (*boxed*). The tree was obtained with the neighbor-joining algorithm of the program ClustalX version 1.64b. Numbers show the values for the bootstrap analysis. SPHKs = sphingosine kinases; CERKs = ceramide kinases; and DGKs = diacylglycerol kinases. Abbreviations and GenBank accession numbers are as follows: human sphingosine kinase 1 (hSPHK1), AAF73423; murine sphingosine kinase 1 (mSPHK1), AAC61697; human sphingosine kinase 2 (hSPHK2), AAF74124; murine sphingosine kinase 2 (mSPHK2), AAF74125; *Drosophila* sphingosine kinase (dSPHK), AAF48045; *Ciona intestinalis* sphingosine kinase (ciSPHK), AK112588; yeast sphingosine kinase Lcb4 (Lcb4p), NP_014814; yeast sphingosine kinase Lcb5 (Lcb5p), NP_013361; *Arabidopsis thaliana* sphingosine kinase (AtSPHK), AY128394; human ceramide kinase (hCERK), AB079066; murine ceramide kinase (mCERK), AB079067; *Ciona intestinalis* ceramide kinase (ciCERK), AK112750; *Drosophila* ceramide kinase (dCERK), AAF52040; human ceramide kinase-like (hCERKL), AY357073; murine ceramide kinase-like (mCERKL), BY742285 and BC046474; *Caenorhabditis elegans* ceramide kinase (cCERK), AAC67466; human diacylglycerol kinase β subunit (hDGKb), Q9Y6T7; murine diacylglycerol kinase β subunit (mDGKb), XP_147651; human diacylglycerol kinase epsilon subunit (hDGKe), NP_003638; murine diacylglycerol kinase epsilon subunit (mDGKe), NP_062378); *Caenorhabditis elegans* diacylglycerol kinase 1 (cDGK1), NP_508190; *Arabidopsis thaliana* diacylglycerol kinase 1 (AtDGK1), Q39017; *Drosophila* diacylglycerol kinase 2 (dDGK2), Q09103; and *Drosophila* diacylglycerol kinase 1 (dDGK1), Q01583.

ceramide kinase (CERK [Sugiura et al. 2002]) (fig. 2) and, therefore, the gene was named "human ceramide kinase–like" (*CERKL* [HUGO-approved nomenclature]). In addition, database searches revealed one murine EST (GenBank accession number BY742285) and one partial cDNA (GenBank accession number BC046474), which, upon assembly and conceptual translation, produced a protein that was highly homologous to human CERKL (75% identity; 85.6% similarity) (fig. 2). To verify that CERKL belonged to the ceramide kinase subfamily of lipid kinases, a phylogenetic tree was constructed using 24 protein sequences from different eukaryotic phyla. Human and murine CERKL sequences clearly clustered within the branch of ceramide kinases (fig. 3).

Premature Truncation of CERKL *Causes arRP*

The *CERKL* coding exons were sequenced in all members of the RP26 family. All patients were homozygous for a nonsense mutation (R257X; CGA→TGA) in exon 5, which prematurely truncates the protein within the predicted catalytic domain (fig. 4*A* and 4*B*). This mutation was not observed in 170 unrelated, ethnically matched control individuals. We subsequently evaluated cosegregation of RP with two *CERKL* flanking markers (D2S2310 and D2S364) in a panel of small nuclear Spanish families with RP whose causative gene was still unknown. An additional cosegregating pedigree, unrelated to the RP26 family, was identified. The *CERKL*

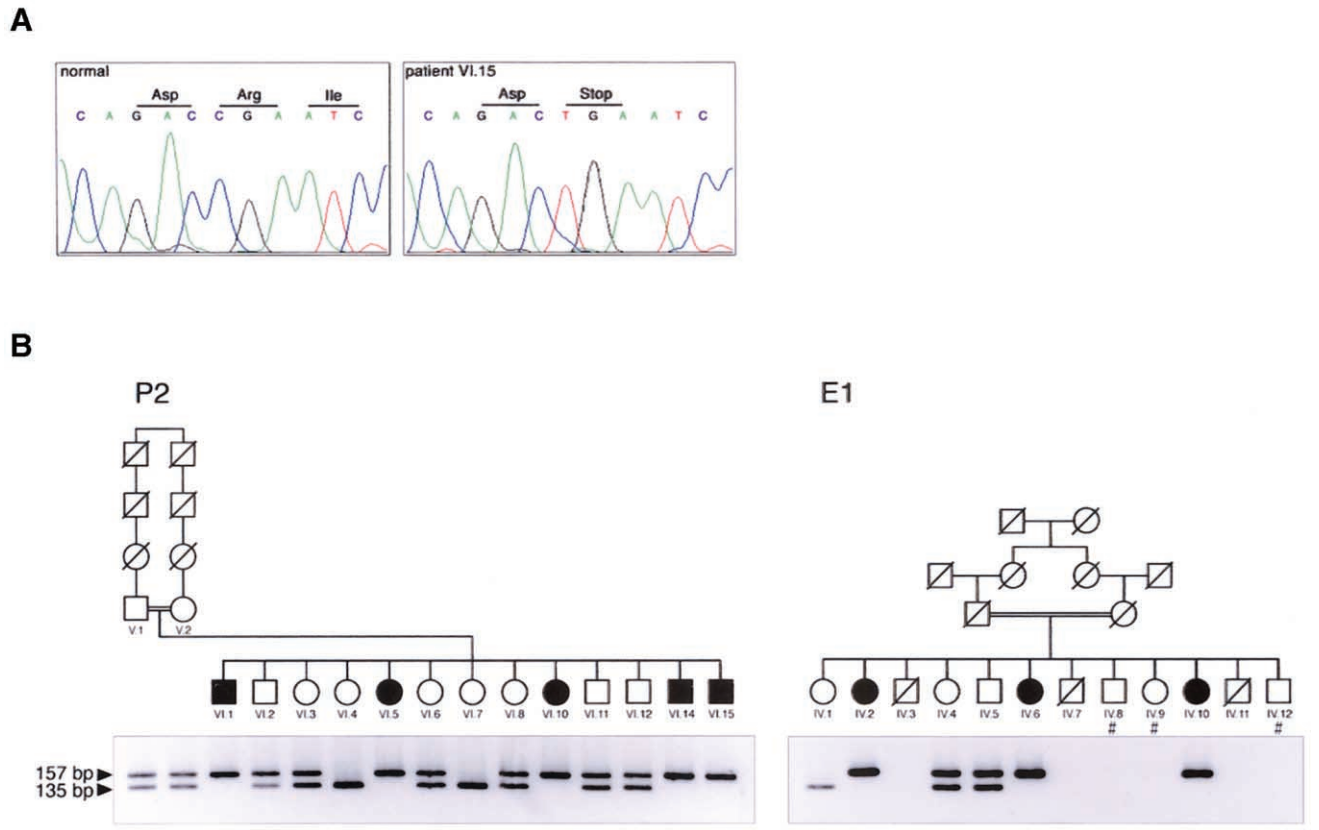

Figure 4 *A,* DNA sequence of exon 5 in an unaffected individual and patient VI.15 of the P2 family, showing the homozygous nonsense R257X mutation. *B,* Pedigrees of P2 and E1 families, showing the ARMS analysis of R257X mutation. A specific primer was designed to generate an *Ava*II restriction site in the amplified wild-type allele. All RP-affected individuals are homozygous for the mutant, nonrestricted allele. Individuals whose DNA samples were not available are indicated by a number sign (#).

sequence analysis showed that the affected members were also homozygous for the R257X mutation (fig. 4*B*), thus reinforcing the pathogenicity of this CERKL variant. Although both families share the same mutation, the haplotype analysis of the 12 nearest flanking markers (see table 1), stretching 600 kb around *CERKL,* does not support a common ancestry (data not shown).

CERKL *Shows a Tissue-Specific Pattern of Expression*

Northern expression analysis of *CERKL* did not reveal any transcript on two panels of several human tissues, even after long exposure times (data not shown). This suggested either specific expression in nontested tissues or very low transcriptional levels, in contrast to the higher and more ubiquitous expression of the *CERK* gene (Sugiura et al. 2002). The more sensitive RT-PCR assays revealed moderate expression in adult human retina, kidney, lung, and pancreas, and low levels in brain, placenta, and liver (fig. 5). The RT-PCRs on human fetal tissues also showed expression in lung, kidney, and brain (fig. 5).

To assess *CERKL* expression in the retina more accurately, we performed in situ hybridization on mouse eye sections. The mouse *CERKL* ortholog is predominantly expressed in the retina ganglion cell layer, although a faint signal is also detected in the inner nuclear and photoreceptor cell layers (fig. 6*A* and 6*B*). The axons from the ganglion cells merge in the optic nerve and, therefore, constitute the last cellular component of phototransduction in the retina.

As a positive control, we assayed rhodopsin, which is highly expressed in the photoreceptor cells (fig. 6*C*). It is remarkable that, at a comparable specific labeling and concentration probe, rhodopsin hybridization signal was much more intense and was detected much earlier than *Cerkl* expression, again supporting the low transcriptional levels of the latter.

Discussion

The identification of *CERKL* and its characterization as an RP causative gene opens new avenues for evaluating

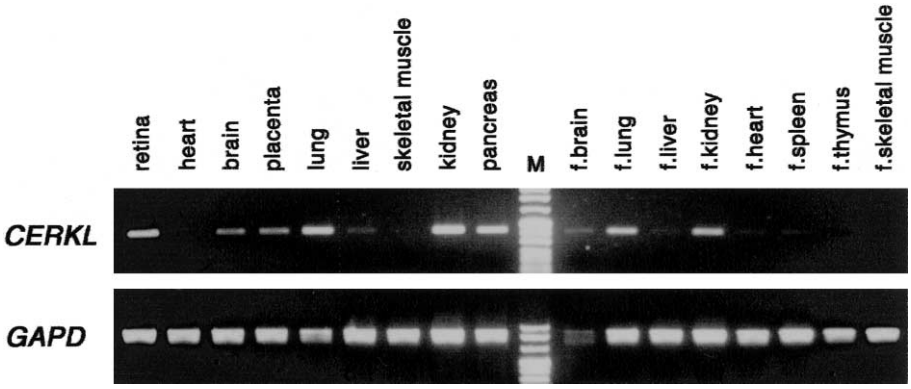

Figure 5 *CERKL* and *GAPD* (control) RT-PCR expression analysis on several human tissues, including retina

its contribution—as well as that of other sphingolipid (SL) metabolism enzymes—to retinal function and disease. The pathogenicity of the R257X mutation is supported not only by the absence of this variant in the control population (the test on 340 chromosomes allows the detection of a polymorphism of 1% with 95% statistical confidence [Collins and Schwartz 2002]) but also, and with more relevance to function, by the premature truncation of the protein (position 257 out of 532 aa), well within the strictly conserved catalytic domain of ceramide, sphingosine, and diacylglycerol kinases (fig. 2).

During the last decade and after exhaustive cosegregation analyses using internal and flanking markers of all the reported arRP genes and loci (including RP26), we have identified the causative gene in only 8 (~15%) families out of 52 Spanish pedigrees with arRP. When we consider all our data, *CERKL* (responsible for the disease in two families [present study]) appears to contribute to arRP to a similar extent as other well-known arRP genes, such as *PDE6B* (three families [Bayés et al. 1996]), *TULP1* (one family [Paloma et al. 2000]), *ABCA4* (one family [Martínez-Mir et al. 1998]), and *CNGA1* (one family [Paloma et al. 2002]). Although it is too early to assess the real contribution of *CERKL* to retinal disorders, we surmise that, after this first study, additional families and new mutations will be readily described.

When we consider CERKL function, we should remember that SLs are structural membrane components, particularly abundant in neurons. SL accumulation is associated with severe neurodegenerative disorders (Gaucher, Tay-Sachs, and Niemann-Pick A and B diseases [Buccoliero and Futerman 2003]). Moreover, increasing evidence points to both nonphosphorylated and phosphorylated sphingosine and ceramide as essential second messengers in cellular stress, senescence, growth, and apoptosis (Luberto et al. 2002). SLs and their metabolic products act as biosensors of the cellular state, and the enzymes that regulate SL metabolism appear to be fine-tuned cellular switches, connecting several pathways with antagonistic properties (Hannun and Obeid 2002). Thus, ceramide and sphingosine lead to cell growth arrest and apoptosis, whereas sphingosine-1-phosphate and ceramide-1-phosphate have antiapoptotic and neuroprotective effects (Frago et al. 1998, 2003; Hannun and Obeid 2002; Spiegel and Milstien 2002, 2003). In this context, sensory neuropathies (hereditary sensory neuropathy type 1 [Dawkins et al. 2001]) and other neurodegenerative diseases (Batten disease [Puranam et al. 1999]) have recently been associated with ceramide metabolism enzyme deficiencies. It is puzzling that some key enzymes regulating intracellular ceramide levels have remained elusive (Hannun and Obeid 2002)—for example, the first ceramide kinase to be characterized was reported only recently (Sugiura et al. 2002). However, despite the short lapse of time, data on the function of ceramide-1-phosphate and ceramide kinase in several scenarios have increased, stressing the roles of the relative levels of

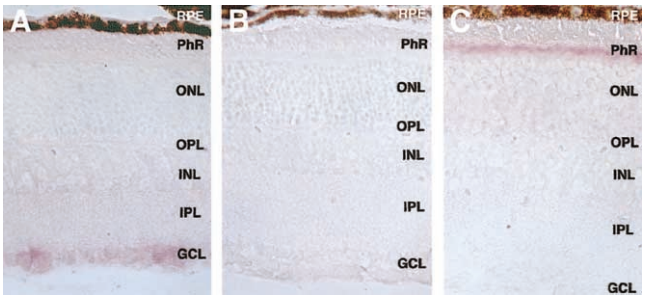

Figure 6 *A, Cerkl* in situ hybridization on murine eye sections with the antisense riboprobe. *B, Cerkl* in situ hybridization on murine eye sections with the sense riboprobe (negative control). *C, Rhodopsin* in situ hybridization on murine eye sections (positive control). RPE = retinal pigment epithelium; PhR = photoreceptor cell layer; ONL = outer nuclear layer; OPL = outer plexiform layer; INL = inner nuclear layer; IPL = inner plexiform layer; GCL = ganglion cell layer.

ceramide and ceramide-1-phosphate as intracellular indicators for cell death/survival decisions (Frago et al. 2003) and adding a prominent role in the regulation/modulation of inflammatory responses (Pettus et al. 2003).

Photoreceptor neurodegeneration in RP has been reported to proceed by apoptosis triggered by cellular stress. However, none of the described genetic defects underlying inherited retinal dystrophies has provided a direct link to apoptosis. It is interesting that a very recent report showed that a decrease of the intracellular ceramide pools rescued photoreceptor degeneration in *Drosophila* mutants (Acharya et al. 2003). Ceramide may be produced in the photoreceptors in response to stress. In this case, deficiency of CERKL, a specific retinal ceramide kinase, would increase the ceramide pool or decrease the ceramide-1-phosphate levels, rendering the photoreceptor cells more susceptible to stress and, thus, more sensitive to apoptotic signals. The cumulative effects of this enhanced susceptibility could lead to progressive depletion of photoreceptors and, eventually, to blindness. Failure to process the ceramide to ceramide-1-phosphate may trigger cell death not only by increasing the endogenous ceramide pool but also by failing to activate the corresponding downstream signalling pathway. Whether *CERKL* is transcriptionally modulated in response to cellular stress stimuli remains an open question.

This study—to our knowledge, the first genetic report linking RP to ceramide-induced apoptosis—highlights the SL metabolism enzymes as new functional candidates and establishes novel targets for therapeutic intervention of retinal diseases.

Acknowledgments

We are indebted to the families with arRP who generously contributed to this study, particularly to all members of the P2 family and to Isabel Tejada from the Hospital General de Basurto (Bilbao, Spain) for providing the E1 family samples. This research followed the tenets of the Convention of Helsinki. We are grateful to Rebeca Valero and Olga Gonzàlez-Angulo, for technical help; to Susana Balcells, for valuable suggestions; and to Robin Rycroft, for revising the English. We thank the Serveis Científico-Tècnics (Universitat de Barcelona) for the sequencing and in situ hybridization facilities. This work was financed by Fundaluce (2001) and by Ministerio de Ciencia y Tecnología grant PM99-0168 (to R.G.-D.). M.T. was in receipt of a Formació d'Investigadors fellowship from the Generalitat de Catalunya.

Electronic-Database Information

Accession numbers and URLs for data presented herein are as follows:

BCM Search Launcher, http://searchlauncher.bcm.tmc.edu/

dbSNP Home Page, http://www.ncbi.nlm.nih.gov/SNP/ (for the new SNPs observed in the present study, which are deposited under the following identification numbers: ss12676100, ss12676101, ss12676102, ss12676103, ss12676104, ss12676105, ss12676106, ss12676107, ss12676108, ss12676109, ss12676110, ss12676111, ss12676112, ss12676113, and ss12676114)

EMBnet BoxShade Server, http://www.ch.embnet.org/software/BOX_form.html

GenBank, http://www.ncbi.nih.gov/Genbank/ (for truncated EST [accession number BE797822], partial cDNA [accession number BC020465], human SPHK1 [accession number AAF73423], murine SPHK1 [accession number AAC61697], human SPHK2 [accession number AAF74124], murine SPHK2 [accession number AAF74125], *Drosophila* SPHK [accession number AAF48045], *C. intestinalis* SPHK [accession number AK112588], yeast Lcb4p [accession number NP_014814], yeast Lcb5p [NP_013361], *A. thaliana* SPHK [accession number AY128394], human CERK [accession number AB079066], murine CERK [accession number AB079067], *C. intestinalis* CERK [accession number AK112750], *Drosophila* CERK [accession number AAF52040], human CERKL [accession number AY357073], murine CERKL [accession numbers BY742285 and BC046474], *C. elegans* CERK [accession number AAC67466], human DGKb [accession number Q9Y6T7], murine DGKb [accession number XP_147651], human DGKe [accession number NP_003638], murine DGKe [accession number NP_062378], *C. elegans* DGK1 [accession number NP_508190], *A. thaliana* DGK1 [accession number Q39017], *Drosophila* DGK2 [accession number Q09103], and *Drosophila* DGK1 [accession number Q01583])

NCBI BLAST, http://www.ncbi.nlm.nih.gov/BLAST/

NCBI Conserved Domain Database, http://www.ncbi.nih.gov/Structure/cdd/cdd.shtml

Online Mendelian Inheritance in Man (OMIM), http://www.ncbi.nlm.nih.gov/Omim/ (for RP)

RetNet, http://www.sph.uth.tmc.edu/RetNet/

SNP Consortium, The, http://snp.cshl.org/

UCSC Genome Bioinformatics Web Site, http://genome.ucsc.edu/

References

Acharya U, Patel S, Koundakjian E, Nagashima K, Han X, Acharya JK (2003) Modulating sphingolipid biosynthetic pathway rescues photoreceptor degeneration. Science 299: 1740–1743

Bayés M, Goldaracena B, Martínez-Mir A, Iragui-Madoz MI, Solans T, Chivelet P, Bussaglia E, Ramos-Arroyo MA, Baiget M, Vilageliu L, Balcells S, González-Duarte R, Grinberg D (1998) A new autosomal recessive retinitis pigmentosa locus maps on chromosome 2q31-q33. J Med Genet 35:141–145

Bayés M, Martínez-Mir A, Valverde D, del Rio E, Vilageliu L, Grinberg D, Balcells S, Ayuso C, Baiget M, Gonzàlez-Duarte R (1996) Autosomal recessive retinitis pigmentosa in Spain: evaluation of four genes and two loci involved in the disease. Clin Genet 50:380–387

Buccoliero R, Futerman AH (2003) The roles of ceramide and complex sphingolipids in neuronal cell function. Pharmacol Res 47:409–419

Collins JS, Schwartz CE (2002) Detecting polymorphisms and mutations in candidate genes. Am J Hum Genet 71:1251–1252

Dawkins JL, Hulme DJ, Brahmbhatt SB, Auer-Grumbach M, Nicholson GA (2001) Mutations in *SPTLC1*, encoding serine palmitoyltransferase, long chain base subunit-1, cause hereditary sensory neuropathy type I. Nat Genet 27:309–312

Frago LM, Cañón S, de la Rosa EJ, León Y, Varela-Nieto I (2003) Programmed cell death in the developing inner ear is balanced by nerve growth factor and insulin-like growth factor I. J Cell Sci 116:475–486

Frago LM, León Y, de la Rosa EJ, Gómez-Munoz A, Varela-Nieto I (1998) Nerve growth factor and ceramides modulate cell death in the early developing inner ear. J Cell Sci 111: 549–556

Hannun YA, Obeid LM (2002) The ceramide-centric universe of lipid-mediated cell regulation: stress encounters of the lipid kind. J Biol Chem 277:25847–25850

Hims MM, Diager SP, Inglehearn CF (2003) Retinitis pigmentosa: genes proteins and prospects. Dev Ophthalmol 37: 109–125

Luberto C, Kraveka JM, Hannun YA (2002) Ceramide regulation of apoptosis versus differentiation: a walk on a fine line. Lessons from neurobiology. Neurochem Res 27:609–617

Martínez-Mir A, Paloma E, Allikmets R, Ayuso C, del Rio T, Dean M, Vilageliu L, Gonzàlez-Duarte R, Balcells S (1998) Retinitis pigmentosa caused by a homozygous mutation in the Stargardt disease gene *ABCR*. Nat Genet 18:11–12

Paloma E, Hjelmqvist L, Bayés M, García-Sandoval B, Ayuso C, Balcells S, Gonzàlez-Duarte R (2000) Novel mutations in the *TULP1* gene causing autosomal recessive retinitis pigmentosa. Invest Ophthalmol Vis Sci 41:656–659

Paloma E, Martínez-Mir A, García-Sandoval B, Ayuso C, Vilageliu L, González-Duarte R, Balcells S (2002) Novel homozygous mutation in the alpha subunit of the rod cGMP gated channel (*CNGA1*) in two Spanish sibs affected with autosomal recessive retinitis pigmentosa. J Med Genet 39: E66

Pettus BJ, Bielawska A, Spiegel S, Roddy P, Hannun YA, Chalfant CE (2003) Ceramide kinase mediates cytokine and calcium ionophore-induced arachidonic acid release. J Biol Chem 278:38206–38213

Puranam KL, Guo WX, Qian WH, Nikbakht K, Boustany RM (1999) CLN3 defines a novel antiapoptotic pathway operative in neurodegeneration and mediated by ceramide. Mol Genet Metab 66:294–308

Spiegel S, Milstien S (2002) Sphingosine 1-phosphate, a key cell signaling molecule. J Biol Chem 277:25851–25854

——— (2003) Sphingosine-1-phosphate: an enigmatic signalling lipid. Nat Rev Mol Cell Biol 4:397–407

Sugiura M, Kono K, Liu H, Shimizugawa T, Minekura H, Spiegel S, Kohama T (2002) Ceramide kinase, a novel lipid kinase: molecular cloning and functional characterization. J Biol Chem 277:23294–23300

Sullivan LS, Daiger SP (1996) Inherited retinal degeneration: exceptional genetic and clinical heterogeneity. Mol Med Today 2:380–386

Thompson JD, Gibson TJ, Plewniha F, Jeanmougin F, Higgins DG (1997) The CLUSTAL_X windows interface: flexible strategies for multiple sequence alignment aided by quality analysis tools. Nucleic Acids Res 25:4876–4882

Wang Q, Chen Q, Zhao K, Wang L, Wang L, Traboulsi EI (2001) Update on the molecular genetics of retinitis pigmentosa. Ophthalmic Genet 22:133–154